analytical chemistry

pubs.acs.org/ac Article

# Nanothorn Filter-Facilitated Online Cell Lysis for Rapid and Deep Intracellular Profiling by Single-Cell Mass Spectrometry

Shu-Ting Xu, Cheng Yang, and Xiu-Ping Yan*

Cite This: *Anal. Chem.* 2021, 93, 15677−15686 Read Online



**ABSTRACT:** Mass spectrometry combined with flow cytometry is emerging for high-throughput single-cell metabolite analysis but still has problems with limited intracellular information coverage. Here, we show a simple and efficient all-in-one system integrating cell injection, cell extraction, online cell lysis, analyte ionization, and mass spectrometric detection for rapid single-HeLa-cell screening with in-depth profiling of cellular metabolites and drugs. Zinc oxide nanothorn-decorated filters with three bore sizes (5.22, 8.36, and 16.75 $\mu$m) were fabricated for efficient online lysis of the cell membrane (even nuclear membrane) to facilitate intracellular analyte release and demonstrated to have a size effect for potential subcellular discrimination. The two smaller-bore filters gave 2−11-fold improvements in signal response for representative intracellular metabolites, such as adenosine, glutamine, and leucine/isoleucine. Especially, the smallest-bore filter enabled successful detection of the metabolites in the nucleus, including tetrahydrobiopterin and cyclic guanosine monophosphate. The developed all-in-one system was explored to monitor the uptake of four anticancer drugs, including 5-fluorouracil, doxorubicin, gambogic acid, and paclitaxel in single cells, and further to investigate the drug uptake trends at the subcellular level. The all-in-one system integrates the merits of high-throughput single-cell screening and in-depth intracellular information profiling and is promising for high-coverage single-cell metabolome analysis to serve cell biology research and cancer research.

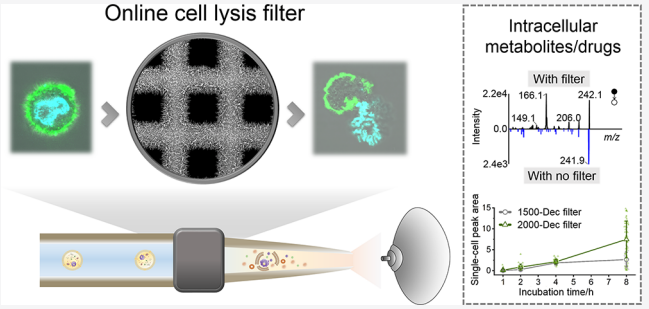




## INTRODUCTION

The diversity and heterogeneity among individual cells are essential for cell differentiation, lesion, and drug resistance in treatment.[1] Measurements at the single-cell level have received increasing attention in cell biology and cancer research in recent years.[2,3] Single-cell metabolome and exogenous drug-related metabolome are direct indicators of cellular activity and cellular response to drug treatment[4,5] but difficult to measure because of their large diversity and impossibility to amplify. Furthermore, the fast dynamic change of metabolome brings great challenges for their real-time measurement in single cells.

Mass spectrometry (MS), owing to the advantages of label-free, information-rich, and high specificity for compound identification, is the most preferred technique for direct monitoring of metabolites and small-molecular drugs in single cells.[6,7] Integrating flexible ionization modes for microvolume-sample analysis gave various single-cell MS methods for *in situ* detection of subcellular metabolites and uptaken drugs,[8] such as live single-cell MS[9] and single-probe MS.[10,11] However, these methods often suffer from the difficulty in manual operation and limited throughput (at least several minutes per cell) for single-cell detection because of indispensable single-cell micromanipulation for sucking up or extracting cellular compounds with capillary tips.

The combination of electrospray ionization (ESI) MS with flow cytometry, such as coupling flow cytometry to ESI-MS (CyESI-MS)[12] and organic mass cytometry,[13] significantly improves the throughput and automation for single-cell detection. These techniques generally reach the cell analysis speeds up to dozens of cells per minute and enable the real-time detection of hundreds of metabolites in intact cells. Nowadays, the flow cytometric single-cell methods present the highest potential to achieve statistically significant single-cell information for cell biology analysis.[14] These real-time flow cytometric MS methods reduce the interference and damage to the native state of cells but have very limited time, space, and specific action for intracellular analytes to release and extract from sampling to ionizing. For these reasons, only a small proportion of compounds mainly from the cell membrane could be detected.[15,16] Considering the whole single-cell information (more than tens of thousands of metabolites), wide coverage of intracellular information is essential for flow cytometric MS analysis.

**Received:** August 17, 2021
**Accepted:** November 1, 2021
**Published:** November 16, 2021




https://doi.org/10.1021/acs.analchem.1c03529
*Anal. Chem.* 2021, 93, 15677−15686

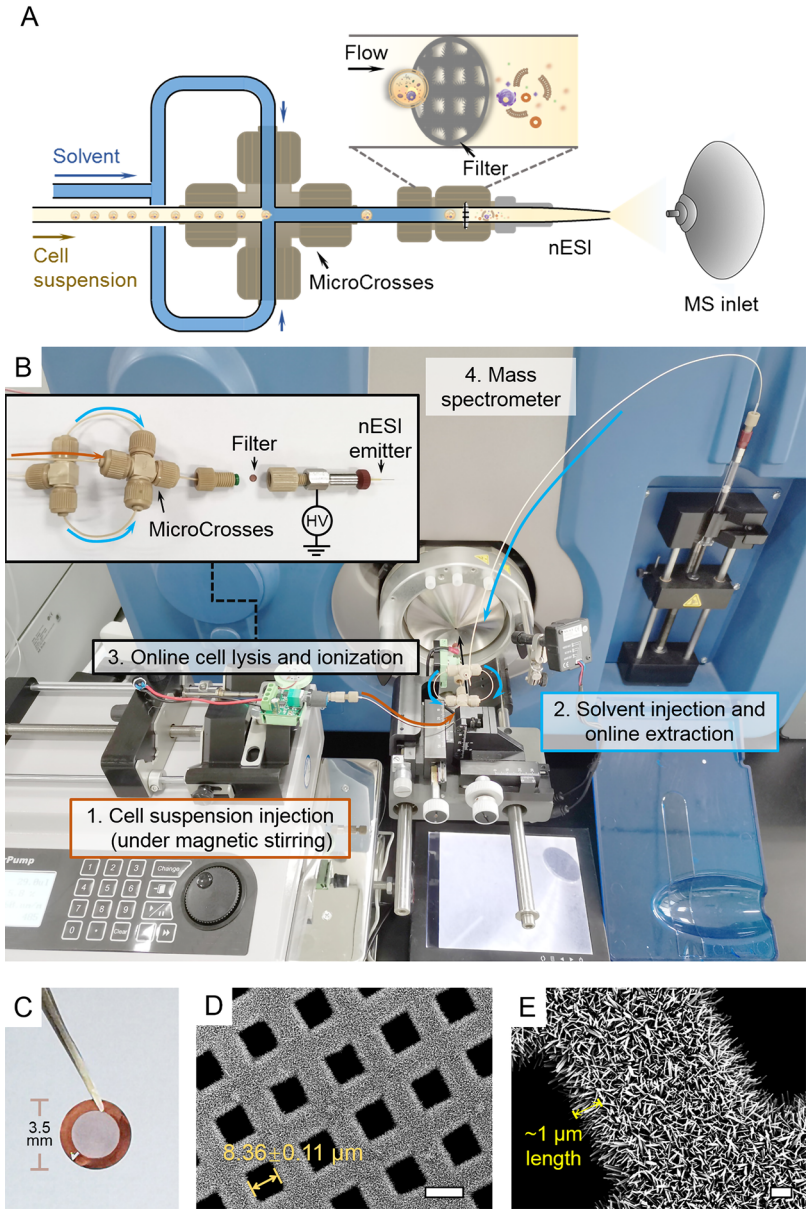


**Figure 1.** Developed all-in-one single-cell system. (A) Schematic diagram of the system. (B) Photo of the all-in-one setup, containing four functional parts: cell suspension injection, solvent injection and online extraction, online cell lysis and ionization, and mass spectrometry. Inset: detailed fittings including the microcrosses for online extraction, a filter for online cell lysis, and a nanoelectrospray ionization (nESI) emitter connected to high voltage for ionization. (C) Photo of a zinc oxide nanothorn (ZnONT)-decorated filter. (D) Scanning electron microscopy (SEM) image of the ZnONT-decorated 1500 mesh grids (scale bar: 10 $\mu$m). (E) Close-up SEM image of the slender and sharp ZnONTs on grids (scale bar: 1 $\mu$m).

Facilitating cell lysis and cellular analyte release during the flow or ionization process is the key to improving intracellular coverage. Chemical, electrical, and mechanical lysis strategies are all candidates for cell lysis and intracellular compound release. Chemical lysis is often utilized for off-line cell pretreatment,[17,18] but it has problems of time consumption and reagent incompatibility with MS. Online chemical lysis only allows the use of MS-compatible organic solvents. The interaction of intact cells with organic solvents in seconds leads to scant cell lysis and sample extraction.[16,19] Specific electric fields, such as high-voltage pulses, can be employed online during ionization to improve intracellular analyte release by cell electroporation but require expensive and complex electrical equipment in addition to mass spectrometry.[20,21]

Mechanical lysis allows reagentless cell lysis with simple devices.[22] In addition, it is easily applied for online cell lysis in a pressure-driven cell flow microsystem using nanostructures.[23−26] Sharp nanostructures, such as nanoscale barbs,[23] nanospikes,[24] and nanowires,[25,26] can efficiently rupture cell membrane online in microchannels or microchips. Microsystems with sharp nanostructures are mostly coupled to optical or electrochemical detectors for cellular protein quantification and nucleic acid detection.[23,25] However, these mechanical lysis strategies have never been utilized in flow cytometric MS systems to improve the intracellular metabolite release so far.

Here, we report an online mechanical lysis strategy for flow cytometric MS systems for rapid and deep intracellular


https://doi.org/10.1021/acs.analchem.1c03529
Anal. Chem. 2021, 93, 15677−15686

profiling. Slender and sharp zinc oxide nanothorns (ZnONTs) are grown on the filter surface for efficient online cell membrane lysis, and the effect of filter bore size on the lysis degree is evaluated. New filters are designed to be compatible with single-cell capillary flow before a nanoelectrospray ionization (nESI) emitter. A versatile all-in-one flow cytometric single-cell analysis system integrating cell injection, extraction, lysis, ionization, and detection is thus established. This system is demonstrated for the profiling of intracellular and intranuclear indicators, metabolites, and drugs in single cervical cancer HeLa cells. This work provides a simple and powerful strategy for deep intracellular MS analysis of intact single cells.

## EXPERIMENTAL SECTION

**Chemicals and Materials.** Zinc oxide nanoparticles (ZnONPs) (<50 nm), branched polyethylenimine (PEI) with average molecular weights of *ca.* 800, and ammonium formate (99.0%) were purchased from Sigma-Aldrich (Shanghai, China). Zinc nitrate hexahydrate ($Zn(NO_3)_2{\cdot}6H_2O$) (AR), hexamethylenetetramine (HMTA) (AR), chloroform (AR), ethanol (AR), *N*,*N*-dimethylformamide (DMF) (AR), and 5-fluorouracil (FU) (BR) were from Sinopharm (Shanghai, China). Vybrant DiO cell-labeling solution (DIO), methanol (high-performance liquid chromatography (HPLC) grade), and acetonitrile (HPLC grade) were from Thermo Fisher Scientific (Shanghai, China). Lyso-Tracker Green (Lyso), Mito-Tracker Green (Mito), and 4% paraformaldehyde fix solution were from Beyotime (Shanghai, China). Heochst 33342 (Heochst) (99%) and rhodamine B (AR) were from Macklin (Shanghai, China). Gambogic acid (GA) (97%) and doxorubicin hydrochloride (DOX) (98%) were from Aladdin (Shanghai, China). Paclitaxel (PTX) (99%) was from InnoChem (Beijing, China). High-purity water was produced by Hangzhou Wahaha Group (Hangzhou, China).

The HeLa cell line was from the cell bank of the Chinese Academy of Sciences (Shanghai, China). Dulbecco's modified Eagle's medium (DMEM) (containing 4.5 g/L D-glucose, L-glutamine and 110 mg/L sodium pyruvate), fetal bovine serum (FBS), penicillin−streptomycin (containing 10 000 unit/mL penicillin and 10 000 μg/mL streptomycin), 0.25% trypsin−ethylenediaminetetraacetic acid (EDTA), and Dulbecco's phosphate-buffered saline (DPBS) were from Gibco (CA).

Copper fine square grids (3.5 mm in diameter and 6 μm of bar width) (G1000HS, 1000 mesh/19 μm bore diameter; G1500HS, 1500 mesh/10.5 μm bore diameter; G2000HS, 2000 mesh/6.5 μm bore diameter) (Gilder Grids, U.K.) were used as the substrates of the online-cell-lysis filters.

**Preparation of ZnONT-Decorated Filters.** The copper grids were washed with ethanol, dried in air, and decorated with ZnONTs in two steps. Ten μL of ZnONPs (0.25 wt % in ethanol) was dropped and spin-coated on the grids. Spin coating was repeated five times for the 1000 mesh grid, four times for the 1500 mesh grid, and three times for the 2000 mesh grid. The ZnONP-coated grids were then rinsed with ethanol for 30 s and immersed in the chemical deposition solution (21 mmol/L $Zn(NO_3)_2$ + 6 mmol/L PEI + 21 mmol/L HMTA) at 90 °C for 3 h to fabricate ZnONTs on the grids. The prepared ZnONT-decorated filters were finally washed with ethanol twice, dried in air, and characterized on a SU8100 scanning electron microscope (SEM) (Hitachi, Japan).

**Setup of the All-in-One Single-Cell System.** The all-in-one single-cell system contained three main functional parts in front of a commercial mass spectrometer QTRAP@4500 (AB SCIEX) (Figure 1A,B): an external syringe pump (LSP02-1B, Longer, China) with a home-made magnetic stirring device for injecting cells, an MS-integrated syringe pump fitted with microcrosses (IDEX) for injecting the solvent and mixing cell flow with solvent flow, and a ZnONT-decorated filter in the flat-bottom connection fittings and connected to the nESI emitter for online cell lysis and analyte ionization (Figures 1B, inset and S1). A fused silica capillary (50 μm i.d. × 150 μm o.d.) was pulled into a tip of about 30 μm on a P-2000 laser-based puller (Sutter Instrument) and cut into a full length of 2.5 cm as the nESI emitter (Figure S1, inset). The parameters of the puller are set as follows: HEAT = 400, FIL = 5, VEL = 28, DEL = 125, and PUL = 80. The polyetheretherketone tubes (65 μm i.d. × 1/32 in. o.d.) were used to connect each functional part. The all-in-one setup was installed in the holder of a Nanospray II Source (P/N #1004600, AB SCIEX) and placed in front of the mass spectrometer. The source holder was equipped with a three-dimensional fine moving platform to control the position of the emitter and a hand-held digital microscope to monitor the emitter area. High voltage, supplied by the MS-integrated high-voltage source and controlled with MS control software, was applied to the nESI emitter through a stainless steel zero-dead-volume adapter.

**Cell Culture.** HeLa cells were cultured in DMEM medium supplemented with 10% FBS, 80 unit/mL penicillin, and 80 μg/mL streptomycin in a 10 cm cell culture dish under 5% $CO_2$ atmosphere at 37 °C. For MS detection and fluorescence imaging, the cells were harvested with 0.25% trypsin−EDTA and centrifuged at 1000 rpm for 4 min. Then, the sediment was resuspended in the medium or DPBS to obtain homogeneous cell suspension for further analysis. The cell number was determined on a Countess 3 automatic cell counter (Thermo Fisher Scientific).

**Subcellular Labeling and Fluorescence Imaging.** The cells were labeled with four subcellular fluorescent dyes, including DIO for membrane labeling, Mito for mitochondria labeling, Lyso for lysosome labeling, and Heochst for nucleus labeling as follows: 1 mL of harvested cells with a concentration of about $10^5$ cells/mL was resuspended in a medium containing 100 nmol/L Lyso and 200 nmol/L Mito. The cell suspension was incubated in the dark at 37 °C with gentle shaking for 25 min. Ten μL of 100 μg/mL Heochst and 1 μL of DIO solution were added to the cell suspension, and the suspension was continued to be incubated in the dark at 37 °C for 10 min with gentle shaking. After labeling, the cells were washed with DPBS five times and finally resuspended in 1 mL of 140 mmol/L ammonium formate aqueous solution (pH 7.3).

The labeled cells seeded in the 20 mm glass-center confocal dish (Biosharp Life Sciences, China) were observed on a Fluoview FV3000 laser scanning confocal microscope (Olympus, Japan). Channel Heochst 33342 (laser wavelength, 405 nm; detection wavelength, 430−470 nm) was selected for Heochst imaging, and channel blue (laser wavelength, 488 nm; detection wavelength, 500−600 nm) was selected for Lyso, Mito, and DIO imaging.

**Test for Online Cell Lysis.** The cell suspension was diluted to a concentration of about $10^4$ cells/mL and detected with the all-in-one system. The flow rates for the cell suspension and solvent were set as 0.6 and 2.4 μL/min, respectively. Methanol was used as the solvent for online extraction with rhodamine B as the internal standard (IS).


https://doi.org/10.1021/acs.analchem.1c03529
Anal. Chem. 2021, 93, 15677−15686

Three MS scan modes including multiple reaction monitoring (MRM), Q1 MS, and product ion (MS2) were employed. The MS parameters for Q1 and MS2 modes are listed in Table S1. Fourteen precursor ion/product ion pairs of the four subcellular fluorescent dyes and IS were monitored in MRM for labeled cells under the optimal conditions in Table S2. Twelve precursor ion/product ion pairs of eight endogenous metabolites and IS were monitored in MRM for unlabeled cells with the conditions in Table S3. For the evaluation of cross-interference between cells, the mixture of Heochst-labeled cells and unlabeled cells was detected by monitoring the ion pairs of Heochst and PC(34:1) (760.8/184.1) in the MRM mode.

The MS instrument and data analysis were controlled with Analyst software (version 1.6.3). Single-cell-peak areas based on the signals of four dye quantitative ion pairs were used to optimize the flow rate conditions and solvents. Single-cell-peak areas based on the calibrated signals of four dye and eight metabolite quantitative ion pairs with IS were employed to evaluate the online cell lysis degree. The calibrated signal intensities of the dye quantitative ion pairs with IS (36 nmol/L rhodamine B) had good linear relationships with dye concentrations (Figure S2 and Table S4).

Online lysed cells were collected on the confocal dish for confocal microscopy imaging. SEM was employed to observe the cells on the filters. Before SEM characterization, the cells were fixed with 4% paraformaldehyde solution for 2 h and dehydrated by ethanol−water solutions with gradient ethanol volume fractions (30, 50, 75, 80, 95, and 100%; each solution for 15 min).

**Analysis of Single-Cell Drug Uptake.** Four anticancer drugs, including FU, DOX, GA, and PTX, were simultaneously incubated with adherent HeLa cells in the medium (about $2 \times 10^6$ cells in each 10 mm dish). Three concentrations (0.8, 0.4, and 0.2 $\mu$g/mL) of each drug were tested. The cells were harvested for different periods (1, 2, 4, and 8 h), and most cells maintained intact morphology for cytometric analysis after drug stimulation (Figure S3). The harvested cells were washed with DPBS four times and resuspended in 140 mmol/L ammonium formate solution to obtain a final concentration of about $10^4$ cells/mL.

The drug-treated cells were detected on the all-in-one system with MRM, Q1, and MS2 modes. Each sample was detected for 15 min. The MS parameters for Q1 and MS2 modes are listed in Table S1. Fourteen precursor ion/product ion pairs of the four drugs and IS were monitored in MRM under the optimal conditions in Table S5. Single-cell-peak areas based on the calibrated signals of four drug quantitative ion pairs with IS were employed to reflect the relative intracellular drug uptake amounts in single HeLa cells for anticancer drug uptake and pharmacokinetics studies. The calibrated signal intensities of the drug quantitative ion pairs with IS (20 nmol/L rhodamine B) had good linear relationships with drug concentrations (Figure S4 and Table S6).

## RESULTS AND DISCUSSION

**Characterization of ZnONTs Decorated on Copper Grids.** Only the shear and frictional forces from flat grids is not sufficient to rupture the mammalian cell membrane because of their certain elasticity (Young's modulus, ~1 kPa).[26,27] Therefore, we fabricated ZnONTs with slender and sharp nanostructures on the microsized girds as online cell lysis filters to rupture the membrane for cell lysis. We employed nanoscale ZnO because of its good mechanical strength, excellent chemical stability, and controllable morphology.[28] Three commercial copper square grids were used as substrates due to appropriate meshes (1000, 1500, and 2000 mesh), sufficient mechanical strength, and compatibility to the flow cytometric MS setup.

Chemical bath deposition was adopted to fabricate ZnONTs because it is a simple and controllable way for nanoscale ZnO growth on solid substrates.[25,28] Taking ZnONT fabricated on 1500 mesh copper grids as an example, 50 nm ZnONPs were coated on copper grids as ZnO seeds to obtain a uniform thin film with a thickness less than 0.6 $\mu$m on grids (Figure S5). The ZnO seeds fully covered the copper surfaces, including the inner surfaces of the bores, and did not significantly change the bore sizes.

Thermal decomposition of $Zn(NO_3)_2$ and HMTA in the PEI aqueous solution further formed ZnONTs on the ZnONP-coated grids. PEI was included in the solution because the absorption of PEI on the ZnO surface could limit the radial growth and guide the axial growth.[29] The concentration of PEI had an obvious effect on the ZnO morphology (Figure S6). PEI with less than 4 mmol/L led to the growth of dense and short ZnO nanowires with blunt hexagon tips (Figure S6A,B). The nanowires are similar to the reported ZnO nanowire arrays for electrical and optoelectronic use[28] but not desired for cell lysis. In contrast, PEI with 6 mmol/L gave preferred slender and sharp nanothorns (ZnONTs) on the grids to provide high potential for cell lysis (Figure S6C). In addition, the ZnONTs on the surface in multiple directions provided multiple angles to penetrate the cell membrane. However, PEI up to 8 mmol/L resulted in only a small number of large ZnO particles (Figure S6D), likely due to the coordination interaction between free $Zn^{2+}$ and exorbitant PEI, and the dissolution of grown ZnO in the alkaline solution. A moderate PEI concentration of 6 mmol/L was finally adopted for ZnONT fabrication, contributing to *ca.* 1.4 $\mu$m thick decorated layer of slender and sharp ZnONTs (*ca.* 1 $\mu$m in length and *ca.* 0.1 $\mu$m in diameter) with multiple directions on the 1500 mesh grids (1500-Dec filter) (Figures 1D,E and S7). After decoration, the 1500-Dec filter maintained an average bore diameter of 8.36 $\mu$m and a porosity of 25.7% (Figure S6C).

The same chemical deposition conditions were successfully expanded to the decoration of ZnONTs on 1000 mesh grids (1000-Dec filter) and 2000 mesh grids (2000-Dec filter) (Figure S8). The 1000-Dec and 2000-Dec filters had 16.75 $\mu$m diameter bores (a porosity of 44.9%) and 5.22 $\mu$m diameter bores (a porosity of 17.4%), respectively.

**All-in-One Configuration for Single-Cell Online Extraction, Lysis, and MS Detection.** Figure 1A,B shows the simple and efficient flow cytometric MS setup integrating single-cell injection, extraction, online lysis, ionization, and MS detection. Flow cytometric mode was preferred to detect intact single cells because of its highest throughput for single-cell analysis.[12,13] The single-cell resolution was obtained by adjusting the concentration of cell suspension and separating cells with microfluidic action in the microchannels.

The cells were injected with low concentrations of about $10^4$ cells/mL to increase the probability of single-cell resolution during MS detection. Continuous magnetic stirring during injection ensured the homogeneous dispersion of the cells. A simple nESI emitter with 30 $\mu$m tip (Figure S1 inset) was employed for ionization. Compared to a typical nESI (1−5


https://doi.org/10.1021/acs.analchem.1c03529
Anal. Chem. 2021, 93, 15677−15686

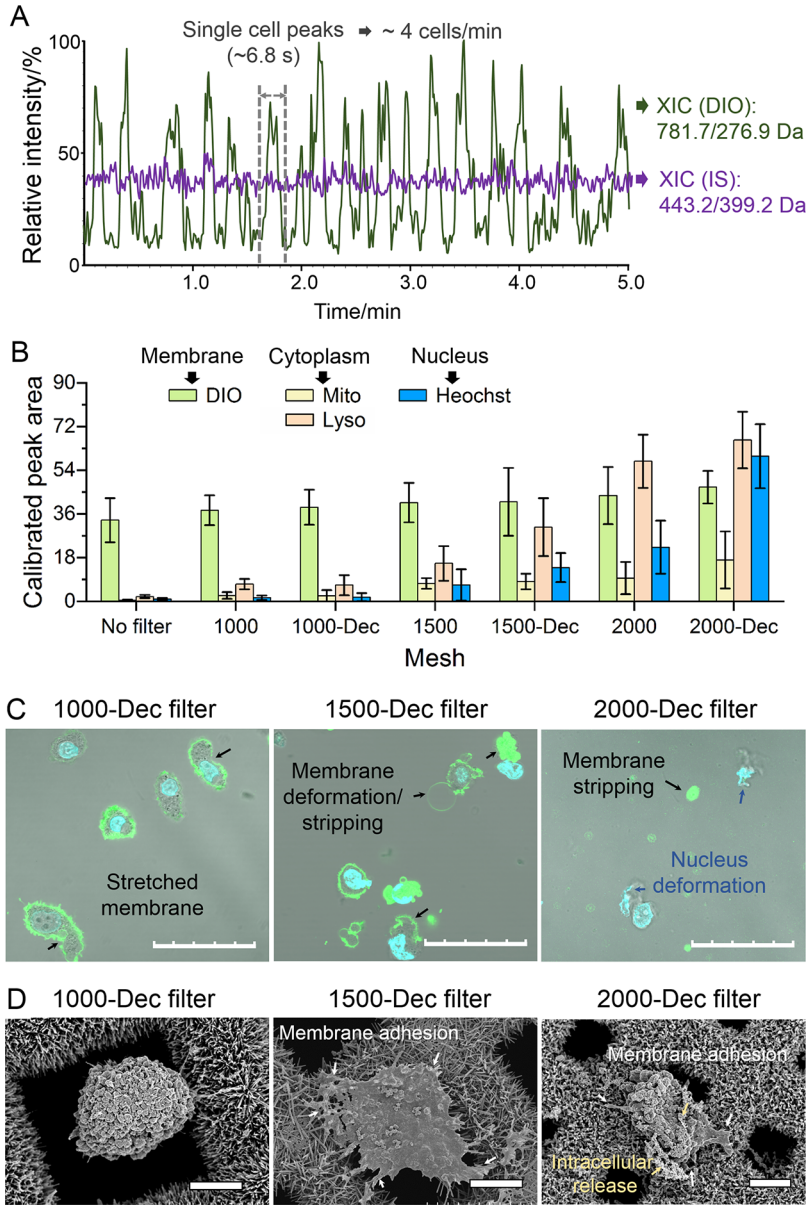


**Figure 2.** (A) Extracted ion chromatograms (XICs) of DIO ion pair (781.7/276.9, green line) and IS ion pair (443.2/399.2, purple line; relative standard deviation (RSD) = 9.6%, $n$ = 18) for the detection of ~$10^4$/mL cells with the 1500-Dec filter (cell suspension, 0.6 $\mu$L/min; methanol, 2.4 $\mu$L/min). (B) Calibrated single-cell peak areas of the four dyes (DIO, Mito, Lyso, and Heochst) acquired on the setup with no filter and the naked/decorated 1000/1500/2000 mesh filters. Error bars: 1 standard deviation for 12 single-cell peaks. (C) Merged bright-field and fluorescence images of HeLa cells labeled with the four dyes after flowing through the 1000/1500/2000 Dec filters (scale bar: 50 $\mu$m). (D) SEM images of fixed cells on the 1000/1500/2000-Dec filters (scale bar: 5 $\mu$m).

$\mu$m), the 30 $\mu$m emitter required higher spray voltage (>3500 V) and matched well with higher flow rates (>1 $\mu$L/min) (Figure S9). Although increasing the emitter size inevitably caused slight loss of sensitivity, a large-size emitter was necessary to avoid tip clogging by cell debris during cytometric analysis.[12,13,30]

Two improved designs of the single-cell system were the use of microcrosses and the addition of online lysis filters between injection and ionization. The microcrosses in the flow system were designed to symmetrically introduce the solvent to the cell suspension. The solvent not only served as the make-up liquid for online extraction and high-efficient ionization of cellular analytes but also acted as the sheath fluid for single-cell focusing and separation.[12,31] In particular, the solvent provided additional force for online cell lysis and reduced sample diffusion. Online cell lysis with the ZnONT-decorated filters was a unique feature of our flow cytometric MS system. The 3.5 mm diameter round filter (Figure 1C) was placed in the flat-bottom connection fittings with good sealing and pressure resisting. Online extraction and lysis were integrated with simple fittings before the nESI emitter. The low-dead-volume connection before ionization could reduce the diffusion of cellular analytes.

Considering the extraction efficiency, lysis degree, and ionization efficiency, important parameters including the total flow rates of the cell suspension and solvent and solvent flow rate proportion were optimized. To clearly show cell lysis degree, HeLa cells were labeled with subcellular localization dyes, including DIO, Mito, Lyso, and Heochst as the indicators of the cell membrane, suborganelles in the cytoplasm and


https://doi.org/10.1021/acs.analchem.1c03529
Anal. Chem. 2021, 93, 15677−15686

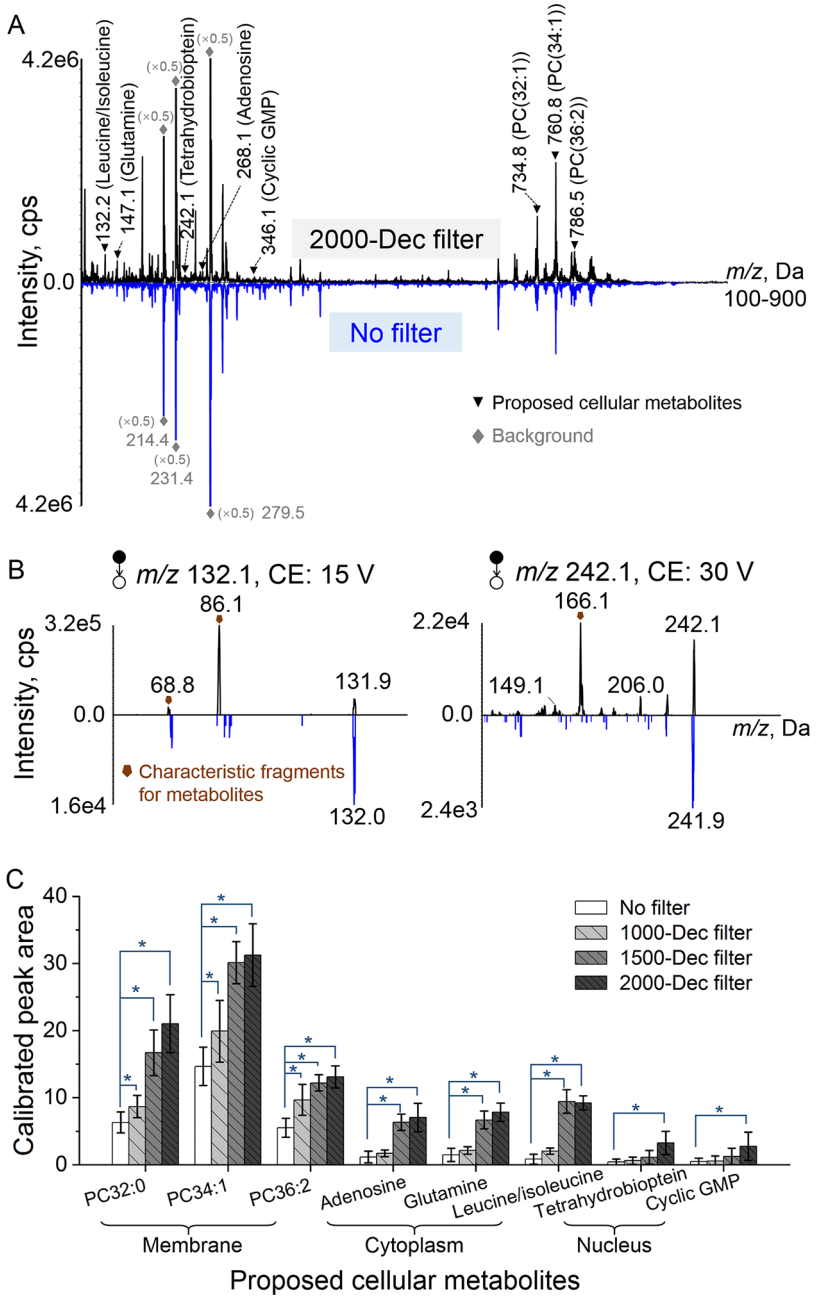


**Figure 3.** (A) Mass spectra of single HeLa cells acquired on the setup with the 2000-Dec filter (black line) and with no filter (blue line). (B) Tandem MS spectra of proposed leucine/isoleucine ($m/z$ 132.1) and tetrahydrobiopterin ($m/z$ 242.1) acquired with the 2000-Dec filter (black line) and with no filter (blue line). (C) Calibrated single-cell peak areas of the eight cellular endogenous metabolites obtained on the setup with no filter and the 1000/1500/2000-Dec filters. Error bars: 1 standard deviation for 12 single-cell peaks (*$P$ < 0.05).

nucleus, respectively. Subcellular organelles were lightened with obvious spatial differentiation under a confocal microscope (Figure S10). The four dyes were simultaneously monitored in MS. The total flow rates adapted to the large-size emitter from 1 to 5 $\mu$L/min with five increasing solvent flow rate proportions (50, 60, 70, 80, and 90%) were tested. Methanol was first introduced as a solvent. About $10^4$ cells/mL of labeled cells gave discrete single-cell peaks in the ion chromatograms with all tested flow rates (Figures 2A, green line and S11). Considering the cellular heterogeneity, 12 single-cell peaks at each condition were averaged to present the trends during optimization. Increasing the flow rate proportion of methanol from 50 to 80% caused the significant enhancement in accumulated signals (Figure S12), so high proportions of solvent were preferred for extraction efficiency and ionization. Theoretically, a lower flow rate of methanol should be better to reduce the sample dilution and achieve a high signal response. In fact, accumulated signals increased from the 1 to 3 $\mu$L/min total flow rates with a certain methanol flow rate proportion (Figures S12 and S13A) because higher total flow rates are beneficial to increase cell lysis degree. Total flow rates from 1 to 3 $\mu$L/min gave obvious higher signals of intracellular dyes including Lyso, Mito, and Heochst due to increased cell lysis and analyte release (Figure S13B). High total flow rates also reduced sample diffusion, from the 26.8 s for one single-cell-peak duration with a total flow rate of 1 $\mu$L/min to the 2.2


https://doi.org/10.1021/acs.analchem.1c03529
Anal. Chem. 2021, 93, 15677−15686

s duration with a total flow rate of 5 μL/min (Figure S11). Overall, the moderate total flow rate of 3 μL/min (cell suspension, 0.6 μL/min; methanol, 2.4 μL/min) was chosen for subsequent experiments to provide the highest single-cell sensitivity. With 6.8 s single-cell duration in this condition and the scan rates in a commercial mass spectrometer (4 s/scan for Q1 and 0.42 s/scan for MRM), an acceptable throughput of about 4 cells/min was obtained (Figure 2A).

Besides methanol, two other MS-compatible solvent compositions with different polarities including methanol/DMF and methanol/water/chloroform were tested. Four subcellular dyes from DIO to Heochst with decreasing calculated log *P* values presented different signal responses with the three solvents (Figure S14A). Considering the accumulated signal response of the four subcellular dyes (Figure S14B), methanol was still a better solvent for analysis.

**Performance of ZnONT-Decorated Filters for In-Depth Intracellular Detection.** The effect of the filter on online lysis of HeLa cells labeled with DIO, Lyso, Mito, and Heochst was investigated. The use of 1500-Dec and 2000-Dec filters facilitated cell lysis and intracellular analyte release. The 1500-Dec filter gave average 13- and 2-fold enhancements of the signals of intracellular Lyso, Mito, and Heochst compared with no filter and naked filter, respectively (Figure S15A). The 2000-Dec filter led to average 20- and 2.5-fold enhancements of the three intracellular signals compared with no filter and naked filter, respectively (Figure S15B). The results showed that the use of the filter and the decoration of slender and sharp ZnONTs obviously improve cell lysis.

The effect of the bore size of ZnONT-decorated filters on cell lysis was further evaluated (Figure 2B). Limited intracellular signals were obtained with the 1000-Dec filter, similar to the results without the filter, due to the larger bores (about 17 μm) on the filter than globular HeLa cells (less than 15 μm) for free passing of intact cells. The 1500-Dec and 2000-Dec filters were more efficient for cell lysis to achieve higher intracellular signals. Furthermore, the 2000-Dec filter with about 5 μm bores enabled the deepest cell lysis to achieve the highest intracellular dye signals and even had the potential for the lysis of the nuclear membrane of HeLa cells. As a result, the 2000-Dec filter gave a more than 4-fold increase in the signal of the nuclear Heochst compared with the 1500-Dec filter.

The lysed cells were imaged on a confocal microscope to observe the change in cellular morphology. The cells almost maintained their intact cellular morphology with the naked 1000 mesh filter (Figure S16, left), while the membranes of some large cells were stretched by the 1000-Dec filter due to the interaction with the ZnONTs on the filter (Figure 2C, left). The little lysis of cells led to the relatively low intercellular signals for MS detection. In contrast, smaller-bore filters even without decoration made the cell membrane partly deform or shed from the nucleus due to the extrusion forces (Figure S16, middle and right). The decorated smaller-bore filters (1500-Dec and 2000-Dec) led to more severe cell morphological destruction as the complete shedding of the membrane from the nucleus (Figure 2C, middle and right), which was consistent with the increase of intracellular signals in MS detection. Furthermore, the nuclear membrane was punctured and the nucleus was deformed on the 2000-Dec filter, contributing to the analyte release from the cell nucleus during MS detection (Figure 2C, right). The cellular morphological changes observed on the microscope demonstrated the performance of decorated smaller-bore filters for efficient deformation and shedding of the cell membrane. The cells on the decorated filters were further captured, fixed, and monitored on SEM to provide a direct observation of the cells interacting with the ZnONTs on girds. Similarly, very limited interaction with cells was observed on the 1000-Dec filter, whereas increased cell lysis was observed on the 1500-Dec and 2000-Dec filters (Figure 2D). Cell membranes were adhered to and stretched by the tips of the ZnONTs in all directions. The deepest cellular morphologic damage and intracellular release were achieved with the 2000-Dec filter.

The performance of ZnONT-decorated filters was further demonstrated for in-depth monitoring of cellular endogenous metabolites in single HeLa cells. Eight metabolites including glycerophosphocholine PC(32:0), PC(34:1), PC(36:2), adenosine, glutamine, leucine/isoleucine, tetrahydrobiopterin, and cyclic guanosine monophosphate (cyclic GMP) in the single-cell spectra (Figure 3A) were focused and identified (Figure S17).

These metabolites showed bore-size-dependent signal response on the ZnONT-decorated filters due to their different subcellular locations (Figure 3C). Phosphatidylcholines (PCs) are key components of the cellular lipid bilayer membrane and the most commonly detectable single-cell compounds in MS.[15,16] The ZnONT-decorated filters gave about 2-fold enhancement of the signals of PCs compared to no filter due to the more efficient extraction of the intracellular membrane after cell lysis. Nucleosides and amino acids usually exist in the cytoplasm or inside the subcellular organelles, especially the mitochondria and lysosomes. Two-to-eleven-fold enhancement of the signals of several intracellular metabolites, such as adenosine, glutamine, and leucine/isoleucine, was achieved with the 1500-Dec and 2000-Dec filters (Figure 3B). Furthermore, tetrahydrobiopterin[32] and cyclic GMP[33] in the nucleus that are difficult to be detected in many existing single-cell methods were successfully detected and identified with the 2000-Dec filter (Figure 3B). The above results show that the 1500-Dec and 2000-Dec filters facilitated the sensitive detection of intracellular analytes in the flow cytometric MS system, especially the 2000-Dec filter further improved the sensitivity and coverage for intranuclear analysis.

As the prerequisite for semiquantitative analysis, the interference from cell residue on the filter during cytometric analysis was evaluated. A mixture of Heochst-labeled cells and unlabeled cells was detected with different filters. Taking the most likely contaminated 2000-Dec filter as an example, the signal of Heochst from the labeled cells rapidly returned to the baseline and had almost no effect on the subsequent unlabeled cells within 15 min (Figure S18A). Although few amount of the residue was observed on the filters by SEM (Figure S18B), the signals of residue were considered as the raised background noise. The background noise was negligible for the semiquantitation based on single-cell peak areas. More residues of the cell content would remain on filters after more cells passed through, and then, the filter required additional washing steps. To ensure minimal residue interference and efficient cytometric analysis, each sample was tested for 15 min. Negligible residue and good ZnONT morphology were also observed for the 1000-Dec and 1500-Dec filters after 15 min use (Figure S19), further supporting the good performance of these ZnONT-decorated filters for online cytometric analysis and accurate semiquantitative analysis.

**Deep Intracellular Drug Profiling in Single HeLa Cells.** The developed all-in-one system was applied for high-


https://doi.org/10.1021/acs.analchem.1c03529
Anal. Chem. 2021, 93, 15677−15686

throughput and deep intracellular drug profiling in single cancer cells. Cellular variations in uptake and response of anticancer drugs are highly concerned in drug resistance research and cancer therapy.[3,34] However, real-time detection of many anticancer drugs *via* flow cytometric MS techniques is challenging because of their intracellular or intranuclear sites of action. The ZnONT-decorated filters integrated into our system enable the efficient release of drugs in the cytoplasm and nucleus for deep single-cell drug profiling applications. To this point, four commonly used anticancer drugs, including FU, DOX, GA, and PTX, were focused in single HeLa cells. Information of more than 50 cells was collected on the all-in-one system with the 1500-Dec filter and 2000-Dec filter for each incubation, and information of a total of more than 1200 single cells was obtained (Table S7).

Significant cellular drug uptake heterogeneity was observed in single HeLa cells for the four anticancer drugs. Drug signals of homologous cells in the same drug exposure condition showed large fluctuation with the RSDs mostly larger than 50% after calibration with IS signals (Table S7) due to different cell cycles, cell states, or drug-resistant individuals. It is noteworthy that a few cells still presented almost no drug uptake until the longest 8 h incubation period with the highest 0.8 $\mu$mol/L drugs (Figures 4A and S20). These cells were highly probable to be drug-resistant or multidrug-resistant cells that could prevent drugs from entering into cells or quickly convert or degrade drugs in cells.[35]

Preliminary pharmacokinetic behaviors of the four anticancer drugs in HeLa cells within 8 h were discussed. Although individual cells presented obvious differences in drug uptake, they still gave obvious trends for intracellular anticancer drug uptake within the 8 h incubation time (Figures 4B,C, S21, and S22). DOX mainly intercalates into the DNA bases in the nucleus,[36] so the 2000-Dec filter was first employed for the detection of intranuclear drugs. Both 0.4 and 0.8 $\mu$mol/L DOX presented accelerated uptake within 8 h (Figures S22B, green line and 4B, green line). FU had a similar trend to DOX (Figures S21A, black line and S22A, black line). As a new anticancer drug, GA presents strong anticancer activity, but its antitumor mechanism has not been clearly studied.[37] The single-cell GA uptake behavior found in this work could assist the GA mechanism study. Because 0.8 $\mu$mol/L GA presented accelerated drug uptake within 8 h (Figure 4C, blue line) and 0.4 $\mu$mol/L GA presented decelerated drug uptake (Figure S22C, blue line), GA might have different drug uptake kinetic mechanisms at different concentrations. The 0.8 $\mu$mol/L PTX showed special uptake behavior of rapid decline after 4 h (Figure S21B, red line). However, this is not the case for 0.4 $\mu$mol/L PTX (Figure S22D, red line). The concentration-dependent uptake of PTX might be attributed to the special PTX uptake mechanism. Since PTX has been demonstrated to reversibly bind to microtubules with concentration dependence,[38] one possible explanation for the decline of PTX amounts in HeLa cells at high incubation concentrations might be its binding to microtubules in cells. The above pharmacokinetic analysis provides a preliminary insight into the molecular mechanism of the four anticancer drugs.

The size effect of 1500-Dec and 2000-Dec filters further provides the opportunity to monitor drug uptake with subcellular discrimination. Different drug signals were obtained with the two filters. Obvious higher drug uptake amounts were obtained at 8 h with the 2000-Dec filter compared to those with the 1500-Dec filter for DOX (Figure 4B) and FU (Figure S21A). The results show the intranuclear uptake of DOX or FU after 4 h incubation with 0.8 $\mu$mol/L drugs. The intranuclear uptake of DOX or FU was not detected with 0.4 $\mu$mol/L drugs within 8 h likely due to the slow intranuclear diffusion of these two drugs.[39] For PTX, the trends were similar for the 1500-Dec filter and 2000-Dec filter at the two concentrations (Figures S21B and S22D) due to the acting sites of PTX on microtubules in the cytoplasm. These results highlight the ability of 1500-Dec and 2000-Dec filters to discriminate the analytes in the cytoplasm and nucleus. Therefore, we proposed the possible intranuclear uptake of 0.8 $\mu$mol/L GA after 4 h because GA presented higher drug uptake amounts acquired with the 2000-Dec filter compared to 1500-Dec filters from 4 to 8 h (Figure 4C). These results provide information on the intracellular behavior of GA to understand the mechanism for inhibition on tumor cell proliferation and induction of apoptosis.[37]

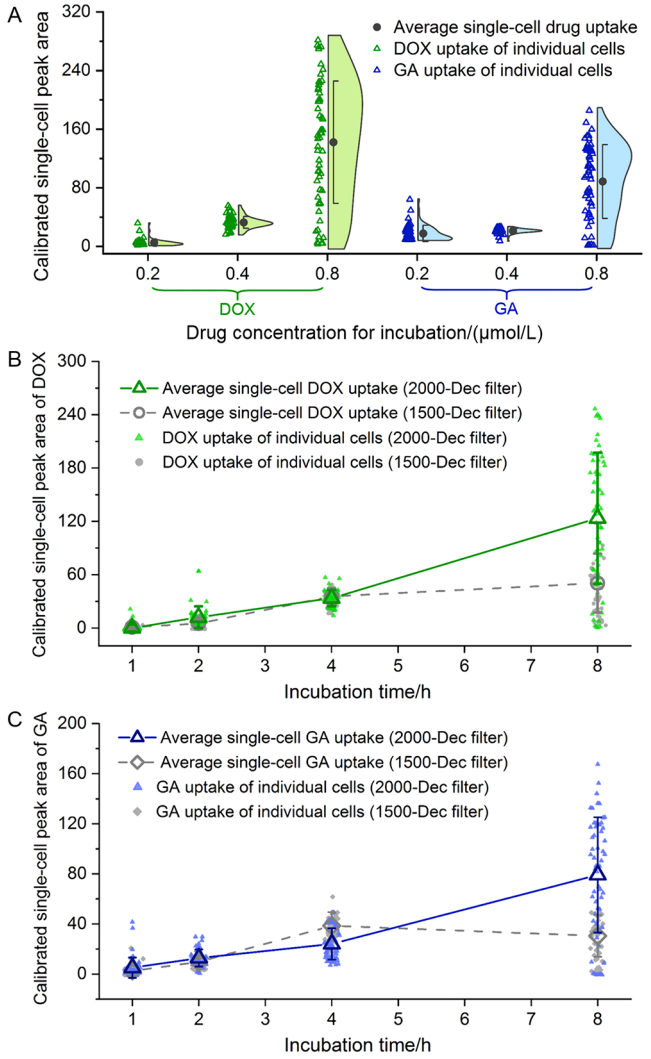


**Figure 4.** (A) Half-violin plots of doxorubicin (DOX) and gambogic acid (GA) uptake in single HeLa cells with three drug concentrations (0.2, 0.4, and 0.8 $\mu$mol/L) for 8 h incubation acquired on the all-in-one setup with the 2000-Dec filter. Uptake of (B) 0.8 $\mu$mol/L DOX and (C) 0.8 $\mu$mol/L GA for individual HeLa cells and average uptake trends within 8 h acquired on the setup with the 2000-Dec filter (color lines) and 1500-Dec filter (gray dot lines). Error bars: 1 standard deviation for more than 50 single-cell peaks. The calibrated single-cell peak area reflects the relative drug uptake amount.


https://doi.org/10.1021/acs.analchem.1c03529
Anal. Chem. 2021, 93, 15677−15686

## CONCLUSIONS

In summary, we have developed an all-in-one single-cell-analysis system with advantages of single-cell sensitivity, high throughput, simple operation, and deep intracellular profiling. Integrating specially designed ZnONT-decorated filters to flow cytometric nESI-MS allows efficient online release of intracellular and intranuclear analytes and provides a powerful solution to solve the problem of limited information coverage. The bore size effect of the filters provides additional opportunities to discriminate analytes from the cytoplasm and nucleus. The developed all-in-one single-cell-analysis system has been successfully applied for the analysis of intracellular and intranuclear metabolites and drugs in single HeLa cells. The obtained abundant deep single-cell information is very helpful for understanding cell behavior and drug uptake mechanisms at the single-cell and subcellular levels. As a universal and powerful single-cell system, it is promising for the in-depth untargeted single-cell metabolome and drug metabolome analysis to serve basic cell biology research, drug mechanism research, cancer therapy research, and so on.

## ASSOCIATED CONTENT

### Supporting Information

The Supporting Information is available free of charge at https://pubs.acs.org/doi/10.1021/acs.analchem.1c03529.

Additional tables and figures for the MS parameters, characterization of filters, optimization results of parameters of the all-in-one single-cell system, characterization of lysed cells on the filter, total ion chromatograms and extracted ion chromatograms of discrete single-cell peaks, tandem MS spectra of eight intracellular metabolites, and MS detection results of the four anticancer drugs in single HeLa cells (PDF)

## AUTHOR INFORMATION


### Corresponding Author

**Xiu-Ping Yan** − *State Key Laboratory of Food Science and Technology, Jiangnan University, Wuxi 214122, China; International Joint Laboratory on Food Safety, Wuxi 214122, China; Institute of Analytical Food Safety, School of Food Science and Technology and Key Laboratory of Synthetic and Biological Colloids, Ministry of Education, Jiangnan University, Wuxi 214122, China;* orcid.org/0000-0001-9953-7681; Email: xpyan@jiangnan.edu.cn

### Authors

**Shu-Ting Xu** − *State Key Laboratory of Food Science and Technology, Jiangnan University, Wuxi 214122, China; International Joint Laboratory on Food Safety, Wuxi 214122, China; Institute of Analytical Food Safety, School of Food Science and Technology and Key Laboratory of Synthetic and Biological Colloids, Ministry of Education, Jiangnan University, Wuxi 214122, China*

**Cheng Yang** − *State Key Laboratory of Food Science and Technology, Jiangnan University, Wuxi 214122, China; International Joint Laboratory on Food Safety, Wuxi 214122, China; Institute of Analytical Food Safety, School of Food Science and Technology and Key Laboratory of Synthetic and Biological Colloids, Ministry of Education, Jiangnan University, Wuxi 214122, China*

Complete contact information is available at: https://pubs.acs.org/10.1021/acs.analchem.1c03529


### Notes

The authors declare no competing financial interest.

## ACKNOWLEDGMENTS

This work was financially supported by the National Natural Science Foundation of China (Nos. 22104044 and 21775056), the China Postdoctoral Science Foundation (No. 2021M691270), the National First-class Discipline Program of Food Science and Technology (No. JUFSTR20180301), and the Collaborative Innovation Center of Food Safety and Quality Control in Jiangsu Province.

## REFERENCES


(1) Franklin, S. *Nature* **2020**, *579*, 339−340.
(2) Buenrostro, J. D.; Corces, M. R.; Lareau, C. A.; Wu, B.; Schep, A. N.; Aryee, M. J.; Majeti, R.; Chang, H. Y.; Greenleaf, W. J. *Cell* **2018**, *173*, 1535−1548.
(3) Bendall, S. C.; Simonds, E. F.; Qiu, P.; Amir, E.-a. D.; Krutzik, P. O.; Finck, R.; Bruggner, R. V.; Melamed, R.; Trejo, A.; Ornatsky, O. I.; Balderas, R. S.; Plevritis, S. K.; Sachs, K.; Pe'er, D.; Tanner, S. D.; Nolan, G. P. *Science* **2011**, *332*, 687−696.
(4) Wang, D.; Bodovitz, S. *Trends Biotechnol.* **2010**, *28*, 281−290.
(5) Zenobi, R. *Science* **2013**, *342*, No. 1243259.
(6) Comi, T. J.; Do, T. D.; Rubakhin, S. S.; Sweedler, J. V. *J. Am. Chem. Soc.* **2017**, *139*, 3920−3929.
(7) Neumann, E. K.; Do, T. D.; Comi, T. J.; Sweedler, J. V. *Angew. Chem., Int. Ed.* **2019**, *58*, 9348−9364.
(8) Yang, Y.; Huang, Y.; Wu, J.; Liu, N.; Deng, J.; Luan, T. *TrAC, Trends Anal. Chem.* **2017**, *90*, 14−26.
(9) Fujii, T.; Matsuda, S.; Tejedor, M. L.; Esaki, T.; Sakane, I.; Mizuno, H.; Tsuyama, N.; Masujima, T. *Nat. Protoc.* **2015**, *10*, 1445−1456.
(10) Pan, N.; Rao, W.; Kothapalli, N. R.; Liu, R.; Burgett, A. W. G.; Yang, Z. *Anal. Chem.* **2014**, *86*, 9376−9380.
(11) Pan, N.; Standke, S. J.; Kothapalli, N. R.; Sun, M.; Bensen, R. C.; Burgett, A. W. G.; Yang, Z. *Anal. Chem.* **2019**, *91*, 9018−9024.
(12) Yao, H.; Zhao, H.; Zhao, X.; Pan, X.; Feng, J.; Xu, F.; Zhang, S.; Zhang, X. *Anal. Chem.* **2019**, *91*, 9777−9783.
(13) Xu, S.; Liu, M.; Bai, Y.; Liu, H. *Angew. Chem., Int. Ed.* **2021**, *60*, 1806−1812.
(14) Benoist, C.; Hacohen, N. *Science* **2011**, *332*, 677−678.
(15) Zhang, W.; Li, N.; Lin, L.; Huang, Q.; Uchiyama, K.; Lin, J.-M. *Small* **2020**, *16*, No. 1903402.
(16) Huang, Q.; Mao, S.; Khan, M.; Li, W.; Zhang, Q.; Lin, J.-M. *Chem. Sci.* **2020**, *11*, 253−256.
(17) Zhu, Y.; Clair, G.; Chrisler, W. B.; Shen, Y.; Zhao, R.; Shukla, A. K.; Moore, R. J.; Misra, R. S.; Pryhuber, G. S.; Smith, R. D.; Ansong, C.; Kelly, R. T. *Angew. Chem., Int. Ed.* **2018**, *57*, 12370−12374.
(18) Chen, Q.; Yan, G.; Gao, M.; Zhang, X. *Anal. Chem.* **2015**, *87*, 6674−6680.
(19) Cahill, J. F.; Riba, J.; Kertesz, V. *Anal. Chem.* **2019**, *91*, 6118−6126.
(20) Li, G.; Yuan, S.; Zheng, S.; Liu, Y.; Huang, G. *Anal. Chem.* **2018**, *90*, 3409−3415.
(21) Li, Z.; Wang, Z.; Pan, J.; Ma, X.; Zhang, W.; Ouyang, Z. *Anal. Chem.* **2020**, *92*, 10138−10144.
(22) Islam, M. S.; Aryasomayajula, A.; Selvaganapathy, P. R. *Micromachines* **2017**, *8*, No. 83.
(23) Di Carlo, D.; Jeong, K.-H.; Lee, L. P. *Lab Chip* **2003**, *3*, 287−291.
(24) So, H.; Lee, K.; Seo, Y. H.; Murthy, N.; Pisano, A. P. *ACS Appl. Mater. Interfaces* **2014**, *6*, 6993−6997.
(25) So, H.; Lee, K.; Murthy, N.; Pisano, A. P. *ACS Appl. Mater. Interfaces* **2014**, *6*, 20693−20699.
(26) Yasui, T.; Yanagida, T.; Shimada, T.; Otsuka, K.; Takeuchi, M.; Nagashima, K.; Rahong, S.; Naito, T.; Takeshita, D.; Yonese, A.;

Magofuku, R.; Zhu, Z.; Kaji, N.; Kanai, M.; Kawai, T.; Baba, Y. *ACS Nano* **2019**, *13*, 2262−2273.
(27) Brody, J. P.; Han, Y. Q.; Austin, R. H.; Bitensky, M. *Biophys. J.* **1995**, *68*, 2224−2232.
(28) Vayssieres, L. *Adv. Mater.* **2003**, *15*, 464−466.
(29) Hu, X.; Masuda, Y.; Ohji, T.; Kato, K. *Appl. Surf. Sci.* **2009**, *255*, 6823−6826.
(30) Huang, Q.; Mao, S.; Khan, M.; Zhou, L.; Lin, J.-M. *Chem. Commun.* **2018**, *54*, 2595−2598.
(31) Dai, Y.; Li, C.; Yi, J.; Qin, Q.; Liu, B.; Qiao, L. *Anal. Chem.* **2020**, *92*, 8051−8057.
(32) Thony, B.; Laufs, S.; Resibois, A.; Leimbacher, W.; Blau, N. *Am. J. Hum. Genet.* **2001**, *69*, 475.
(33) Simmons, D. V.; Petko, A. K.; Paladini, C. A. *J. Neurophysiol.* **2017**, *118*, 1998−2008.
(34) Lawson, D. A.; Kessenbrock, K.; Davis, R. T.; Pervolarakis, N.; Werb, Z. *Nat. Cell Biol.* **2018**, *20*, 1349−1360.
(35) Kartal-Yandim, M.; Adan-Gokbulut, A.; Baran, Y. *Crit. Rev. Biotechnol.* **2016**, *36*, 716−726.
(36) Sritharan, S.; Sivalingam, N. *Life Sci.* **2021**, *278*, No. 119527.
(37) Liu, Y.; Chen, Y.; Lin, L.; Li, H. *Int. J. Nanomed.* **2020**, *15*, 10385−10399.
(38) Zhu, L.; Chen, L. *Cell. Mol. Biol. Lett.* **2019**, *24*, No. 40.
(39) Decorti, G.; Peloso, I.; Favarin, D.; Klugmann, F. B.; Candussio, L.; et al. *J. Pharmacol. Exp. Ther.* **1998**, *286*, 525−530.


https://doi.org/10.1021/acs.analchem.1c03529
*Anal. Chem.* 2021, 93, 15677−15686